PHOTONICS Research

Single-mode helical Bragg grating waveguide created in a multimode coreless fiber by femtosecond laser direct writing

Jun He,[1,2] Jia He,[1,2] Xizhen Xu,[1,2] Bin Du,[1,2] Baijie Xu,[1,2] Changrui Liao,[1,2] Zhiyong Bai,[1,2] and Yiping Wang[1,2,*]

[1]Key Laboratory of Optoelectronic Devices and Systems of Ministry of Education/Guangdong Province, College of Physics and Optoelectronic Engineering, Shenzhen University, Shenzhen 518060, China
[2]Shenzhen Key Laboratory of Photonic Devices and Sensing Systems for Internet of Things, Guangdong and Hong Kong Joint Research Centre for Optical Fibre Sensors, Shenzhen University, Shenzhen 518060, China
*Corresponding author: ypwang@szu.edu.cn

We demonstrate the fabrication of single-mode helical Bragg grating waveguides (HBGWs) in a multimode coreless fiber by using a femtosecond laser direct writing technique. This approach provides a single-step method for creating Bragg grating waveguides. Specifically, the unique helical structure in such an HBGW serves as a depressed cladding waveguide and also generates strong Bragg resonance due to its periodicity. Effects of pulse energy, helical diameter, and helical pitch used for fabricating HBGWs were studied, and a single-mode HBGW with a narrow bandwidth of 0.43 nm and a Bragg wavelength of 1546.50 nm was achieved by using appropriate parameters, including a diameter of 10 µm and a helical pitch of 1.07 µm. The measured cross-sectional refractive index profile indicates that a depressed cladding waveguide has been created in this single-mode HBGW. Moreover, five single-mode HBGWs with various Bragg wavelengths were successfully fabricated by controlling the helical pitch, and this technique could be used for achieving a wavelength-division-multiplexed HBGW array. Then, the temperature and strain responses of the fabricated single-mode HBGW were tested, exhibiting a temperature sensitivity of 11.65 pm/°C and a strain sensitivity of 1.29 pm/µε, respectively. In addition, the thermal stability of the single-mode HBGW was also studied by annealing at a high temperature of 700°C for 15 h. The degeneration of the single-mode waveguide into a multimode waveguide was observed during the isothermal annealing process, and the peak reflection and the Bragg wavelength of the fundamental mode exhibited a decrease of ~7 dB and a "blue" shift of 0.36 nm. Hence, such a femtosecond laser directly written single-mode HBGW could be used in many applications, such as sapphire fiber sensors, photonic integrated circuits, and monolithic waveguide lasers. © 2021 Chinese Laser Press

https://doi.org/10.1364/PRJ.434719

1. INTRODUCTION

Bragg gratings have been playing vital roles in modern optics and photonics. They are formed by a series of submicrometer-scale periodic structures created in optical fiber or planar waveguides and are widely used as optical filters or reflectors in many areas, such as optical networks, fiber lasers, fiber sensors, and all-optical signal processors [1–4]. The femtosecond laser direct-writing technique is a powerful tool for creating functional devices (such as gratings and waveguides) inside transparent optical materials due to its ultrashort pulse duration, ultrahigh peak intensity, and high flexibility in device patterning [5–8]. The femtosecond laser introduces localized micromodification in single crystals, bulk glasses, optical fibers, or semiconductor chips, and can result in permanent refractive index

changes in these optical materials. As such, Bragg gratings consisting of periodic refractive index modulation structures could be created by using such a femtosecond laser direct-writing method [8]. This method exhibits significant advantages in the fabrication flexibility and stability over other Bragg grating fabrication methods. For example, the femtosecond laser phase-mask method is widely used for producing high-quality fiber Bragg gratings (FBGs). However, it is difficult to fabricate Bragg gratings with various wavelengths or complex spectral shapes by using one phase mask [9–11]. Another approach for Bragg grating inscription is based on a femtosecond laser Talbot interferometer, which can be developed for fabricating a wavelength-division-multiplexed (WDM) FBG array by tuning the included angle of incident beams [12,13].

However, the fabrication process requires both high stability and high accuracy, as the extremely short pulse width requires a path difference within a few micrometers [12]. Consequently, the femtosecond laser direct-writing technique becomes the most promising way for Bragg grating inscription and has been widely studied at present. To date, several femtosecond laser direct-writing methods (point-by-point [14–16], line-by-line [17–20], plane-by-plane [21], continuous core scanning [22], using filaments [23,24]) have been demonstrated for fabricating various high-quality single-mode Bragg gratings, including specialty Bragg gratings with complex spectral shapes (i.e., apodized [25], chirped [26], phase-shifted [27], and sampled gratings [28]).

Multimode waveguides, especially multimode fibers (MMFs), are deployed in many scientific and industrial applications, such as astronomical signal filtering [3], spatial-division-multiplexed (SDM) transmission [29], high-energy supercontinuum generation [30], single-fiber imaging [31], 3D holographic optical manipulation [32], and high temperature sensing (based on multimode single-crystal sapphire fibers) [33]. In general, Bragg gratings in MMFs typically have a poor spectral quality with broadened reflection peaks due to the multimode coupling in MMFs [33,34]. The broad reflection peaks in Bragg gratings will either deteriorate the sensing accuracy [18] or reduce the filtering fineness [35]. However, how to create high-quality Bragg gratings in MMFs remains an obstacle. Hence, a single-mode Bragg grating waveguide (BGW), which consists of a Bragg grating and a single-mode optical waveguide, was proposed to overcome this problem. For example, in 2006, the researchers at Macquarie University fabricated a single-mode BGW by writing a single-mode waveguide in bulk fused silica at first and then writing a second-order Bragg grating on the waveguide [36]. Subsequently, in 2007, the researchers at the University of Toronto achieved a first-order BGW via a single-scan writing process by modulating a high-repetition-rate femtosecond fiber laser with an external modulator [37]. This approach was then developed for creating single-mode BGWs with complex refractive index profiles, such as phase-shifted, chirped, and apodized BGWs [38–40]. Note that these single-mode BGWs are Type I waveguides located at the laser-induced tracks, which were formed by positive refractive index changes. Moreover, beam-shaping methods based on additional optical setups [i.e., slit, cylindrical lenses, grating pairs, and spatial light modulators (SLMs)] have been proposed to create symmetric waveguides with circular cross sections, which is beneficial for improving the transmission properties of the waveguide [41–44].

Type II waveguides, based on negative refractive index changes, have also been widely studied [7]. A conventional strategy for fabricating Type II waveguides is to construct depressed claddings in various geometries (i.e., double lines, multiple lines, and ring-shaped layer), which are fabricated via multiple scans [45–51]. The double-line-based waveguide can merely support the propagation of a certain polarization mode [45,46]. Moreover, the optical confinement can be enhanced by adding more tracks in the cladding layer [47–51]. Nevertheless, it is time-consuming for inscribing a large number of tracks. Therefore, a femtosecond laser direct-writing method with a consecutive helical trajectory was proposed for rapid fabricating of Type II waveguides, in which fully enclosed cross sections could be obtained [52,53]. In addition, a single-scan direct-writing method with annular ring-shaped focal intensity distribution was reported for efficient fabrication of Type II waveguides [54]. In general, Type II waveguides can have improved transmission loss and thermal stability [5,7]. However, there are no reports on the fabrication of a Type II single-mode BGW at present.

In this paper, we report for the first time, to the best of our knowledge, a new method for creating Type II single-mode BGWs by using femtosecond laser direct writing in a single-scan process with a helical trajectory. The inscribed helical structure serves both as a depressed cladding waveguide and as a Bragg grating, and leads to a helical BGW (HBGW). The influences of pulse energy, helical diameter, and helical pitch for fabricating HBGWs were studied, and a single-mode HBGW was achieved in a multimode coreless fiber after optimizing the writing parameters. The cross-sectional refractive index profile of the HBGW indicates a depressed cladding waveguide has been created in the fabricated HBGW. Moreover, single-mode HBGWs with various pitches were also fabricated by using this method. Hence, a WDM HBGW array can be achieved. In addition, the temperature and strain responses of the HBGWs were also tested, exhibiting a temperature sensitivity of 11.65 pm/°C and a strain sensitivity of 1.29 pm/με. And then, a long-term high-temperature study of the fabricated single-mode HBGW was performed, and the result shows that the fundamental mode cannot withstand a high temperature of 700°C.

2. DEVICE FABRICATION AND CHARACTERIZATION

As shown in Fig. 1, the proposed HBGW device was fabricated by using an Yb:KGW [KGd(WO$_3$)] femtosecond laser (Pharos, Light Conversion) with a wavelength of 514 nm, a pulse width of 290 fs, and a repetition rate of 200 kHz as the laser source. A 63× Zeiss oil-immersion objective with a numerical aperture (N.A.) of 1.40 was used as the focusing element. Note that the objective with a higher N.A. is beneficial for the formation of symmetric refractive index changes. Moreover, a commercial multimode coreless silica fiber
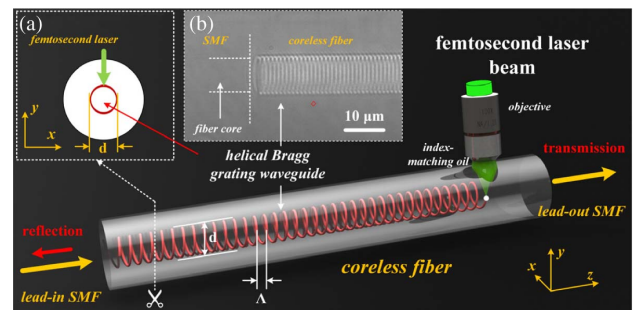

Fig. 1. Schematic of an HBGW created in coreless fiber by femtosecond laser direct-writing technique. Insets: (a) schematic in cross-sectional view of the HBGW; (b) side-view microscope image of a fabricated HBGW sample with a diameter of 10 μm.

(Thorlabs, FG125LA) was used for fabricating HBGWs. Such a coreless fiber is made of pure silica. And then, the refractive index matching oil was applied between the coreless fiber and objective to reduce the aberration at the silica/air interface. An assembled three-axis air-bearing translation stage (Aerotech, ABL15010, ANT130LZS, and ANT130V-5) was used to precisely translate the coreless fiber.

The process for fabricating an HBGW in the coreless fiber is also illustrated in Fig. 1. At first, the coreless fiber with a length of 2 mm was spliced with two segments of single-mode fiber (SMF, Corning, G652D). Then, the spliced coreless fiber was mounted on the 3D translation stage with a pair of fiber holders. The axial direction of the coreless fiber was adjusted parallel to the translation along the z axis. Subsequently, the shutter was opened, and the femtosecond laser beam was focused into the coreless fiber. In this process, the coreless fiber was translated in a helical trajectory via synchronous movements along the x, y, and z axes, and a helical structure was hence created in the coreless fiber. As shown in the inset (a) of Fig. 1, the cross section of the helical structure is annular, which serves as a depressed cladding. Moreover, as shown in the inset (b) of Fig. 1, the helical trajectory provides a periodic structure with a diameter of 10 μm and a helical pitch of 1.07 μm, which can yield a second-order Bragg grating resonance in the telecommunication C-band.

We characterized the optical properties, including the near-field profile of transmission mode, reflection spectra, and polarization-resolved transmission spectra, of the fabricated HBGWs by using the experimental setup illustrated in Fig. 2. At first, the near-field profiles of transmission mode in HBGWs were measured by using the optical path 1. A linearly polarized laser beam was generated from a tunable laser (Keysight, 81940A, with central wavelength set to be 1547.50 nm) and a polarization synthesizer (Keysight, N7786B) and incident on the sample under test. A mode observation system consisting of lens and CCD (Newport, LBP2-HR-IR2) was set up to measure the near-field profiles. A variable optical attenuator (VOA) was used to avoid saturation of infrared CCD pixels. And then, the reflection spectra of HBGWs were measured by using the optical path 2, which consists of a tunable laser and an optical power meter (Keysight, N7744A). The polarization-resolved transmission spectra of HBGWs were measured by using the optical path 3, i.e., a Muller-matrix-based polarization analyzer consisting of a tunable laser, a polarization synthesizer, and an optical power meter.
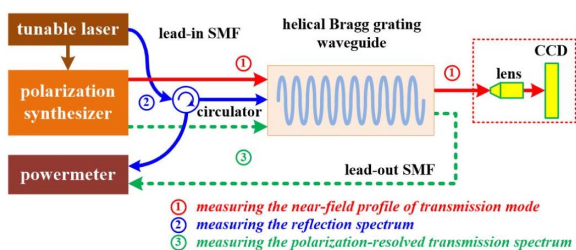
At first, we fabricated three HBGW samples, S1, S2, and S3, with decreasing helical diameters of 30, 20, and 10 μm using the same pulse energy of 26.5 nJ. These HBGWs have the same helical pitch of 1.07 μm and the same length of 2 mm. As shown in Figs. 3(a1)–3(a3) and 3(b1)–3(b3), ring-shaped inscription patterns have been created in the fabricated HBGW cross sections, and periodic Bragg grating structures can be seen from the side view. In the case of S1 [HBGW with a large diameter of 30 μm, as shown in Figs. 3(a1) and 3(b1)], multimode operation could be seen from the near-field profile of the transmission mode shown in Fig. 3(c1) and the reflection spectrum shown in Fig. 3(d1), in which a Bragg resonance with a broad −3 dB bandwidth of 1.80 nm is exhibited. Moreover, in the case of S2 [HBGW with a reduced diameter of 20 μm, as shown in Figs. 3(a2) and 3(b2)], higher-order modes could be suppressed partially, and its reflection spectrum exhibits a reduced bandwidth of 0.69 nm, as shown in Fig. 3(d2). Then, in the case of S3 [HBGW with a small diameter of 10 μm, as shown in Figs. 3(a3) and 3(b3)], a pure fundamental mode (LP01) is observed in Fig. 3(c3), and the reflection spectrum exhibits a single-mode Bragg resonance with a narrow bandwidth of 0.43 nm, as shown in Fig. 3(d3). As a result, a single-mode HBGW with a Bragg wavelength of ∼1546.50 nm was successfully created in a multimode coreless fiber.

The polarization-resolved transmission spectra of the fabricated single-mode HBGW sample S3 were studied via the setup shown in path 3 of Fig. 2. As shown in Fig. 4, the transmission spectra of two orthogonal polarization modes (i.e., x and y polarizations) of the HBGW S3 exhibit a Bragg wavelength separation of 102 pm, which corresponds to a birefringence of 9.5×10^{-5}. Moreover, the Bragg dip attenuation in x and y polarizations is 26.49, and 20.94 dB, respectively, which corresponds to a reflectivity of 99.78% and 99.19%. The out-of-band insertion loss in x and y polarizations is 10.28 and 5.44 dB, respectively. Note that the discrepancy in the insertion loss of two orthogonal polarizations may result from the asymmetric refractive index distributions in the fabricated HBGW. Additionally, as shown in the inset of Fig. 3(c3), the near-field profile of transmission mode in the fabricated single-mode HBGW S3 exhibits an area of 15.4 μm × 13.1 μm, which is much larger than that in the lead-in and lead-out SMF (i.e., ∼10.4 μm × 10.4 μm). Hence, the mode-field diameter mismatch between the SMF and the HBGW S3 generates a large insertion loss in the transmission spectrum, which could be reduced by further optimization.

We measured the refractive index distribution in the fabricated HBGW S3 by using digital holographic microscopy (SHR-1602, index accuracy: 10^{-4}) fabricated by Shanghai University, China. In this equipment, the optimal digital hologram was obtained from the phase projection distribution of the test fiber, and the refractive index distribution in the fiber was calculated by using an angular spectrum theory-based algorithm and a filtered backprojection algorithm [55]. As shown in Fig. 5(a), a step-index profile with positive and negative refractive index changes could be seen in the cross-sectional refractive index distribution. It could be found from Fig. 5(b) that the maximum positive and negative refractive index changes are 2×10^{-3} and -1×10^{-2}, respectively, which could

Fig. 2. Schematics of the experimental setup for characterizing the optical properties, including the near-field profile of transmission modes, reflection spectra, and polarization-resolved transmission spectra, of the fabricated HBGWs.
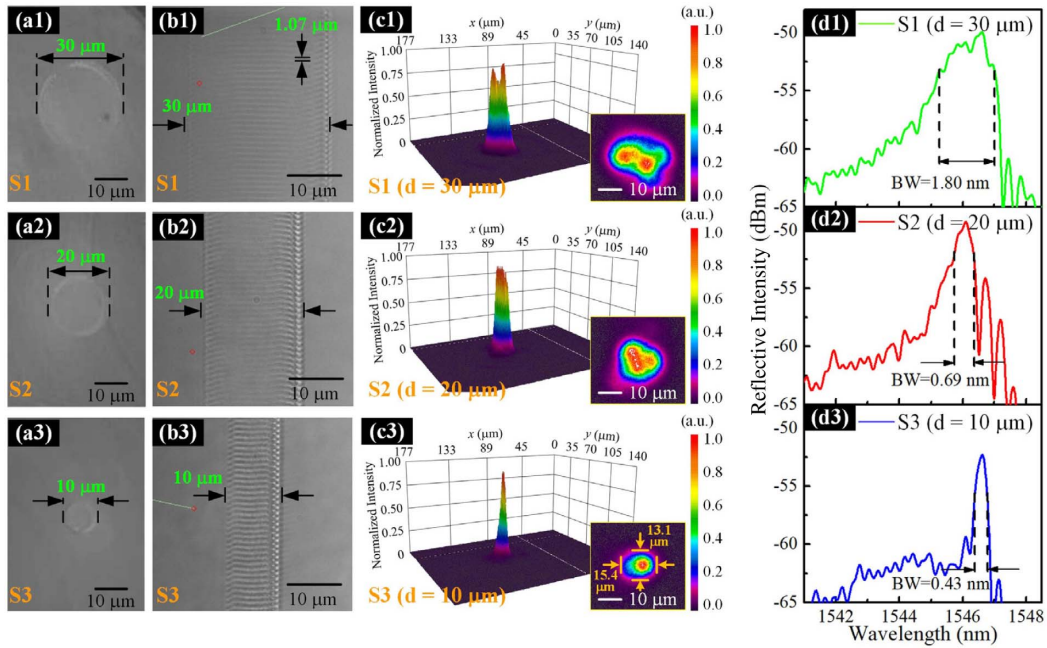
Fig. 3. Microscope images, transmission modes, and reflection spectra of three fabricated HBGW samples S1, S2, and S3 with decreasing diameters of 30, 20, and 10 μm, respectively. (a) Cross-sectional and (b) side view microscope images of S1–S3; (c) near-field profiles of transmission mode in S1–S3 at the resonant wavelength of 1547.50 nm; (d) corresponding reflection spectra of S1–S3.
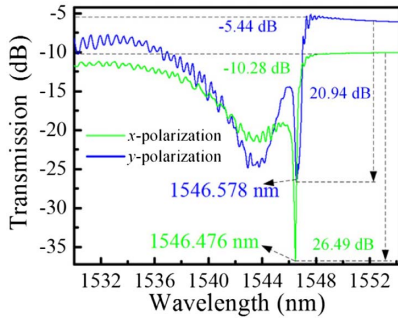

Fig. 4. Transmission spectra of two orthogonal linear polarization modes (x and y) in the single-mode HBGW S3.

ensure the optical confinement in the HBGW. However, as the black dotted circle illustrates in Fig. 5(b), the guiding region is not completely enclosed, and hence leads to a larger insertion
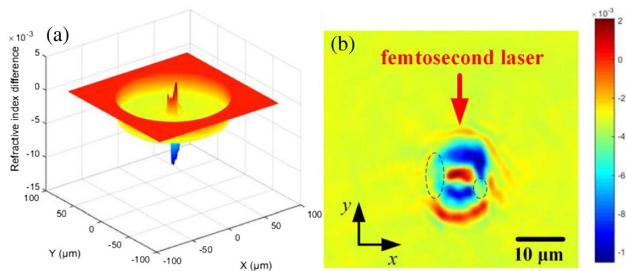

Fig. 5. Refractive index distribution in the cross section of the fabricated single-mode HBGW S3. (a) 3D view and (b) 2D view.

loss in the x polarization. In addition, the cross section of the refractive index changes is not circularly symmetric, which can result in a high birefringence. Moreover, the asymmetric refractive index profile also leads to an increase in cladding mode resonance (including the "ghost" mode, as shown in Fig. 4) [56]. It is obvious that such a refractive index distribution is asymmetric, since the index modulation area created by femtosecond laser direct writing has been elongated along the propagation direction. This problem can be solved by using beam-shaping methods (slits, cylindrical lenses, grating pairs, or SLMs) [41–44].

Subsequently, we fabricated three other HBGW samples (i.e., S4–S6) by using the femtosecond laser helical direct-writing technique with increasing pulse energy of 17.9, 26.5, and 34.1 nJ, respectively. The HBGW samples S4–S6 have the same helical pitch of 1.07 μm, the same helical diameter of 10 μm, and the same grating length of 2 mm. As shown in Figs. 6(a1)–6(a3), the reflectivity increases and the peak wavelength shifts toward a longer wavelength (i.e., a "red" shift) with an increasing writing pulse energy. Note that a single-mode HBGW (i.e., S5) could be achieved only by using appropriate laser pulse energy of 26.5 nJ. Low pulse energy leads to inadequate reflectivity in the HBGW S4 [as shown in Fig. 6(a1)], whereas high pulse energy leads to a broad reflection peak in the HBGW S6 [as shown in Fig. 6(a3)], since a larger refractive index change can result in more propagation modes in the waveguide.

We fabricated three more HBGWs (i.e., S7–S9) with an increasing helical pitch of 1.06, 1.07, and 1.08 μm, respectively. The HBGWs S7–S9 were fabricated by using the same pulse energy of 21 nJ, the same helical diameter of 10 μm, and the same length of 2 mm. As shown in Figs. 6(b1)–6(b3), three

HBGWs exhibit a similar peak reflective intensity of –60 dBm. However, the HBGWs S7 and S8 are in single-mode operation with a narrow bandwidth of 0.32 nm, whereas S9 is in multimode operation with a broad bandwidth of 0.72 nm. Moreover, it should be noted that the higher-order modes located at the shorter wavelengths in the reflection spectrum are significantly increased, as illustrated in Fig. 6(b3). This may result from the decrease in the averaged refractive index in the fabricated HBGW in case the helical pitch was increased, and hence leads to the degeneration from a single-mode waveguide into a multimode waveguide. Consequently, single-mode HBGWs can be created by using appropriate parameters, including a pulse energy of 26.5 nJ, a helical diameter of 10 μm, and a helical pitch of 1.07 μm.

Furthermore, we fabricated single-mode HBGWs with different Bragg wavelengths by simply controlling the helical grating pitches and using appropriate pulse energies. Five single-mode HBGWs (S10–S14) with increasing pitches of 1.04, 1.05, 1.06, 1.07, and 1.08 μm were fabricated by using corresponding pulse energies of 21, 21.5, 23, 26, and 27.5 nJ, respectively. Note that the same helical diameter of 10 μm and the same grating length of 2 mm were used. Moreover, increasing pulse energy was used for inscribing HBGW with an increasing helical pitch, and hence a larger refractive index change could be formed to ensure a single-mode operation
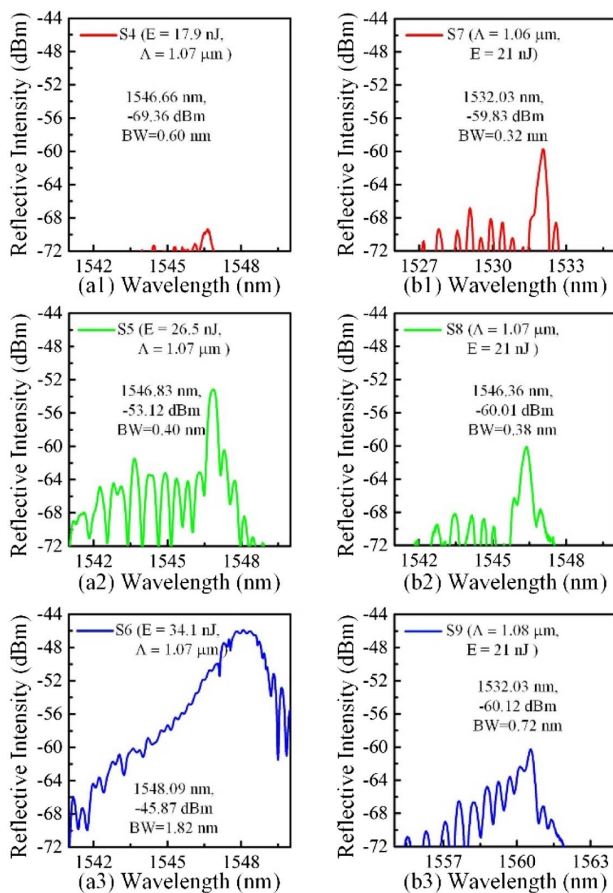
in the HBGW. As shown in Fig. 7, five single-mode HBGWs (S10–S14) are fabricated with distinct Bragg wavelengths of 1503.76, 1517.94, 1532.32, 1546.84, and 1561.39 nm, respectively. Each HBGW exhibits single-mode Bragg resonance with a narrow bandwidth of below 0.5 nm. The results demonstrate the proposed method has an excellent flexibility in tuning the Bragg wavelength like other femtosecond laser direct-writing techniques, and hence could be used for creating a WDM single-mode HBGWs array.

3. TEMPERATURE AND STRAIN RESPONSES

We further investigated the temperature and strain responses of the fabricated single-mode HBGW, which has a helical diameter of 10 μm, a helical pitch of 1.07 μm, and a grating length of 2 mm. The temperature response was evaluated by placing the sample in a high-precision column oven (LCO 102) with an accuracy of 0.1°C. The temperature was varied from room temperature to 100°C and was maintained for 20 min at each measurement point. As shown in Fig. 8(a), the Bragg wavelength of the HBGW exhibits a "red" shift with an increasing temperature and a "blue" shift with a decreasing temperature. The measured temperature sensitivities in the heating and cooling processes are 11.65 and 11.58 pm/°C, respectively. Furthermore, the strain response of the single-mode HBGW was tested by fixing one end of the HBGW and stretching the other end fixed on a translation stage. When the tensile strain applied on the HBGW sample was cycled between 0 and 1000 με, as shown in Fig. 8(b), the Bragg wavelength exhibits a "red" shift with an increasing strain and a "blue" shift
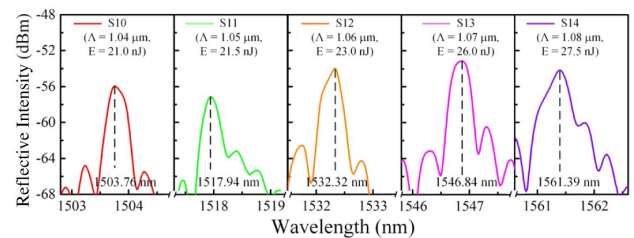
Fig. 7. Five single-mode HBGWs (S10–S14) with distinct Bragg wavelengths fabricated with increasing helical pitches (1.04, 1.05, 1.06, 1.07, and 1.08 μm) and corresponding pulse energies (21, 21.5, 23, 26, and 27.5 nJ).

Fig. 6. (a) Reflection spectra of the HBGWs S4–S6 fabricated with increasing pulse energies, and (b) reflection spectra of the HBGWs S7–S9 fabricated with increasing grating pitches.
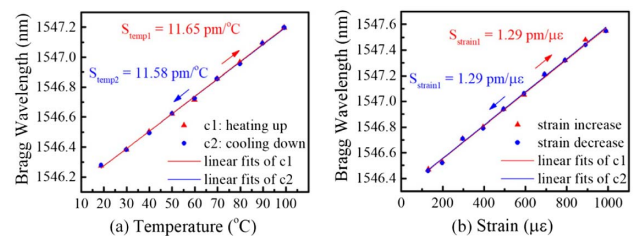
Fig. 8. (a) Measured Bragg wavelength of the fabricated single-mode HBGW as a function of increasing and decreasing temperature ranging from 18 to 100°C, and (b) measured Bragg wavelength of the single-mode HBGW as a function of increasing and decreasing strain ranging from 0 to 1000 με.
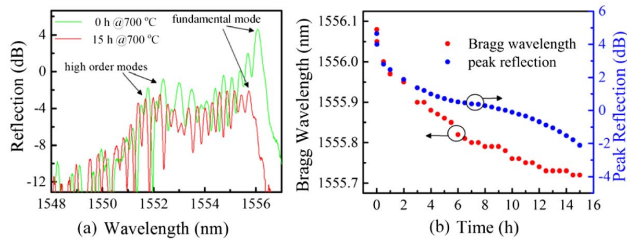
Fig. 9. Long-term isothermal annealing of the fabricated single-mode HBGW at 700°C for 15 h. (a) Reflection spectra of the HBGW before and after long-term annealing at high temperature; (b) evolutions of the measured peak reflection and Bragg wavelength during the annealing process.

with a decreasing strain. The strain sensitivity is 1.29 pm/με. These results agree well with conventional FBGs inscribed on single-mode silica fibers.

Finally, we investigated the thermal stability of the single-mode HBGW via a high temperature test in a tube furnace (Carbolite GERO EHC12-450B). The sample was placed in the furnace center, which has a uniform temperature field within a length of 90 mm and an accuracy of ±5°C. An embedded N-type thermocouple was used to record the temperature. The sample was isothermally annealed at 700°C for 15 h. In the annealing process, the reflection spectra of the sample were measured every 30 min. After annealing at 700°C for 15 h, the Bragg resonance at fundamental mode (i.e., peak wavelength in the reflection spectrum) decreases drastically, but the higher-order mode resonances (at shorter wavelengths in the reflection spectrum) decrease slightly, as shown in Fig. 9(a). Additionally, the peak reflection of the HBGW decreases by ~7 dB and the Bragg wavelength exhibits a "blue" shift of 0.36 nm, as shown in Fig. 9(b). This could be explained by different formation mechanisms and thermal stabilities of two types of refractive index changes [5,57] formed in the fabricated single-mode HBGW, i.e., the negative index change and the positive index change, as shown in Fig. 5(b). Specifically, the negative index change is formed by a femtosecond laser-induced microexplosion, which triggers shock and rarefaction waves and is a permanently damaged area. Such a negative index change can withstand a high temperature. In contrast, the positive index change is formed by the accumulation of internal tensile stress, which can be released via thermal decomposition. Therefore, the positive refractive index change formed inside the helical structure was erased during the high-temperature annealing, leading to a "blue" shift in the Bragg wavelength and the degeneration of the single-mode HBGW into a multimode waveguide.

4. CONCLUSION

We have proposed and demonstrated a novel single-step approach for creating single-mode BGWs based on a helical trajectory directly written in a multimode coreless fiber with a femtosecond laser. The depressed cladding waveguide was formed by the helical structure, and Bragg grating resonance can be generated, since such a device has periodicity. The influences of helical diameter, helical pitch, and pulse energy

on the optical properties of the fabricated HBGWs were experimentally studied, and a single-mode HBGW with a high reflectivity of up to 99.78%, a narrow bandwidth of 0.43 nm, and a Bragg wavelength of 1546.50 nm, was successfully created. Five single-mode HBGWs with different Bragg wavelengths were also fabricated in the coreless fiber. Additionally, the temperature and strain responses of single-mode HBGWs were investigated. Such HBGWs exhibit a temperature sensitivity of 11.65 pm/°C and a strain sensitivity of 1.29 pm/με. Furthermore, the annealing test of single-mode HBGWs shows the fundamental mode cannot withstand a high temperature of 700°C. Therefore, the proposed femtosecond laser helical direct-writing method is very suitable for fabricating single-mode BGWs in many industrial applications, such as multimode sapphire fiber sensors, silicon-based photonic integrated circuits, and monolithic waveguide lasers.

Disclosures. The authors declare no conflicts of interest.

REFERENCES

1. J. Canning, "Fiber gratings and devices for sensors and lasers," Laser Photon. Rev. **2**, 275–289 (2008).
2. G. Gagliardi, M. Salza, S. Avino, P. Ferraro, and P. De Natale, "Probing the ultimate limit of fiber-optic strain sensing," Science **330**, 1081–1084 (2010).
3. J. Bland-Hawthorn, S. C. Ellis, S. G. Leon-Saval, R. Haynes, M. M. Roth, H.-G. Löhmannsröben, A. J. Horton, J.-G. Cuby, T. A. Birks, J. S. Lawrence, P. Gillingham, S. D. Ryder, and C. Trinh, "A complex multi-notch astronomical filter to suppress the bright infrared sky," Nat. Commun. **2**, 581 (2011).
4. W. F. Zhang and J. P. Yao, "A fully reconfigurable waveguide Bragg grating for programmable photonic signal processing," Nat. Commun. **9**, 1396 (2018).
5. M. Beresna, M. Gecevičius, and P. G. Kazansky, "Ultrafast laser direct writing and nanostructuring in transparent materials," Adv. Opt. Photon. **6**, 293–339 (2014).
6. M. Ams, G. D. Marshall, P. Dekker, J. A. Piper, and M. J. Withford, "Ultrafast laser written active devices," Laser Photon. Rev. **3**, 535–544 (2009).
7. F. Chen and J. R. Vázquez de Aldana, "Optical waveguides in crystalline dielectric materials produced by femtosecond-laser micromachining," Laser Photon. Rev. **8**, 251–275 (2014).
8. J. Thomas, C. Voigtländer, R. G. Becker, D. Richter, A. Tünnermann, and S. Nolte, "Femtosecond pulse written fiber gratings: a new avenue to integrated fiber technology," Laser Photon. Rev. **6**, 709–723 (2012).
9. J. He, B. J. Xu, X. Z. Xu, C. R. Liao, and Y. P. Wang, "Review of femtosecond-laser-inscribed fiber Bragg gratings: fabrication technologies and sensing applications," Photon. Sens. **11**, 203–226 (2021).
10. S. J. Mihailov, C. W. Smelser, P. Lu, R. B. Walker, D. Grobnic, H. Ding, and G. Henderson, "Fiber Bragg gratings made with a phase mask and 800-nm femtosecond radiation," Opt. Lett. **28**, 995–997 (2003).
11. K. A. Zagorulko, P. G. Kryukov, Yu. V. Larionov, A. A. Rybaltovsky, and E. M. Dianov, "Fabrication of fiber Bragg gratings with 267 nm femtosecond radiation," Opt. Express **12**, 5996–6001 (2004).

12. M. Becker, J. Bergmann, S. Brückner, M. Franke, E. Lindner, M. W. Rothhardt, and H. Bartelt, "Fiber Bragg grating inscription combining DUV sub-picosecond laser pulses and two-beam interferometry," Opt. Express **16**, 19169–19178 (2008).

13. Z. Zhang, B. J. Xu, J. He, M. X. Hou, W. J. Bao, and Y. P. Wang, "High-efficiency inscription of fiber Bragg grating array with high-energy nanosecond-pulsed laser Talbot interferometer," Sensors **20**, 4307 (2020).

14. A. Martinez, M. Dubov, I. Khrushchev, and I. Bennion, "Direct writing of fibre Bragg gratings by femtosecond laser," Electron. Lett. **40**, 1170 (2004).

15. Y. Lai, K. Zhou, K. Sugden, and I. Bennion, "Point-by-point inscription of first-order fiber Bragg grating for C-band applications," Opt. Express **15**, 18318–18325 (2007).

16. R. J. Williams, N. Jovanovic, G. D. Marshall, G. N. Smith, M. J. Steel, and M. J. Withford, "Optimizing the net reflectivity of point-by-point fiber Bragg gratings: the role of scattering loss," Opt. Express **20**, 13451–13456 (2012).

17. K. M. Zhou, M. Dubov, C. B. Mou, L. Zhang, V. K. Mezentsev, and I. Bennion, "Line-by-line fiber Bragg grating made by femtosecond laser," IEEE Photon. Technol. Lett. **22**, 1190–1192 (2010).

18. X. Z. Xu, J. He, C. R. Liao, K. M. Yang, K. K. Guo, C. Li, Y. F. Zhang, Z. B. Ouyang, and Y. P. Wang, "Sapphire fiber Bragg gratings inscribed with a femtosecond laser line-by-line scanning technique," Opt. Lett. **43**, 4562–4565 (2018).

19. G. Bharathan, T. T. Fernandez, M. Ams, R. I. Woodward, D. D. Hudson, and A. Fuerbach, "Optimized laser-written ZBLAN fiber Bragg gratings with high reflectivity and low loss," Opt. Lett. **44**, 423–426 (2019).

20. G. Bharathan, T. T. Fernandez, M. Ams, J.-Y. Carrée, S. Poulain, M. Poulain, and A. Fuerbach, "Femtosecond laser direct-written fiber Bragg gratings with high reflectivity and low loss at wavelengths beyond 4 μm," Opt. Lett. **45**, 4316–4319 (2020).

21. P. Lu, S. J. Mihailov, H. M. Ding, D. Grobnic, R. B. Walker, D. Coulas, C. Hnatovsky, and A. Y. Naumov, "Plane-by-plane inscription of grating structures in optical fibers," J. Lightwave Technol. **36**, 926–931 (2018).

22. R. J. Williams, R. G. Krämer, S. Nolte, and M. J. Withford, "Femtosecond direct-writing of low-loss fiber Bragg gratings using a continuous core-scanning technique," Opt. Lett. **38**, 1918–1920 (2013).

23. E. Ertorer, M. Haque, J. Z. Li, and P. R. Herman, "Femtosecond laser filaments for rapid and flexible writing of fiber Bragg grating," Opt. Express **26**, 9323–9331 (2018).

24. X. Z. Xu, J. He, J. He, B. J. Xu, R. X. Chen, Y. Wang, Y. T. Yang, and Y. P. Wang, "Efficient point-by-point Bragg grating inscription in sapphire fiber using femtosecond laser filaments," Opt. Lett. **46**, 2742–2745 (2021).

25. R. J. Williams, C. Voigtländer, G. D. Marshall, A. Tünnermann, S. Nolte, M. J. Steel, and M. J. Withford, "Point-by-point inscription of apodized fiber Bragg gratings," Opt. Lett. **36**, 2988–2990 (2011).

26. S. Antipov, M. Ams, R. J. Williams, E. Magi, M. J. Withford, and A. Fuerbach, "Direct infrared femtosecond laser inscription of chirped fiber Bragg gratings," Opt. Express **24**, 30–40 (2016).

27. G. D. Marshall, R. J. Williams, N. Jovanovic, M. J. Steel, and M. J. Withford, "Point-by-point written fiber-Bragg gratings and their application in complex grating designs," Opt. Express **18**, 19844–19859 (2010).

28. C. Z. Zhang, Y. H. Yang, C. Wang, C. R. Liao, and Y. P. Wang, "Femtosecond-laser-inscribed sampled fiber Bragg grating with ultrahigh thermal stability," Opt. Express **24**, 3981–3988 (2016).

29. D. J. Richardson, J. M. Fini, and L. E. Nelson, "Space-division multiplexing in optical fibres," Nat. Photonics **7**, 354–362 (2013).

30. L. G. Wright, D. N. Christodoulides, and F. W. Wise, "Controllable spatiotemporal nonlinear effects in multimode fibres," Nat. Photonics **9**, 306–310 (2015).

31. M. Plöschner, T. Tyc, and T. Čižmár, "Seeing through chaos in multimode fibres," Nat. Photonics **9**, 529–535 (2015).

32. I. T. Leite, S. Turtaev, X. Jiang, M. Šiler, A. Cuschieri, P. St.J. Russell, and T. Čižmár, "Three-dimensional holographic optical manipulation through a high-numerical-aperture soft-glass multimode fibre," Nat. Photonics **12**, 33–35 (2015).

33. X. Z. Xu, J. He, C. R. Liao, and Y. P. Wang, "Multi-layer, offset-coupled sapphire fiber Bragg gratings for high-temperature measurements," Opt. Lett. **44**, 4211–4214 (2019).

34. M. J. Schmid and M. S. Muller, "Measuring Bragg gratings in multimode optical fibers," Opt. Express **23**, 8087–8094 (2015).

35. H. Liang, K. Ying, D. Wang, H. Y. Pi, X. Li, Z. Y. Wang, F. Wei, and H. W. Cai, "All-fiber narrow-bandwidth rectangular optical filter with reconfigurable bandwidth and tunable center wavelength," Opt. Express **29**, 11739–11749 (2021).

36. G. D. Marshall, M. Ams, and M. J. Withford, "Direct laser written waveguide-Bragg gratings in bulk fused silica," Opt. Lett. **31**, 2690–2691 (2006).

37. H. Zhang, S. M. Eaton, and P. R. Herman, "Single-step writing of Bragg grating waveguides in fused silica with an externally modulated femtosecond fiber laser," Opt. Lett. **32**, 2559–2561 (2007).

38. K. Dolgaleva, A. Malacarne, P. Tannouri, L. A. Fernandes, J. R. Grenier, J. S. Aitchison, J. Azaña, R. Morandotti, P. R. Herman, and P. V. S. Marques, "Integrated optical temporal Fourier transformer based on a chirped Bragg grating waveguide," Opt. Lett. **36**, 4416–4418 (2011).

39. J. R. Grenier, L. A. Fernandes, J. S. Aitchison, P. V. S. Marques, and P. R. Herman, "Femtosecond laser fabrication of phase-shifted Bragg grating waveguides in fused silica," Opt. Lett. **37**, 2289–2291 (2012).

40. P. Zeil, C. Voigtländer, J. Thomas, D. Richter, and S. Nolte, "Femtosecond laser-induced apodized Bragg grating waveguides," Opt. Lett. **38**, 2354–2356 (2013).

41. P. S. Salter, A. Jesacher, J. B. Spring, B. J. Metcalf, N. Thomas-Peter, R. D. Simmonds, N. K. Langford, I. A. Walmsley, and M. J. Booth, "Adaptive slit beam shaping for direct laser written waveguides," Opt. Lett. **37**, 470–472 (2012).

42. M. Ams, G. D. Marshall, D. J. Spence, and M. J. Withford, "Slit beam shaping method for femtosecond laser direct-write fabrication of symmetric waveguides in bulk glasses," Opt. Express **13**, 5676–5681 (2005).

43. F. He, H. Xu, Y. Cheng, J. Ni, H. Xiong, Z. Xu, K. Sugioka, and K. Midorikawa, "Fabrication of microfluidic channels with a circular cross section using spatiotemporally focused femtosecond laser pulses," Opt. Lett. **35**, 1106–1108 (2010).

44. G. Cerullo, R. Osellame, S. Taccheo, M. Marangoni, D. Polli, R. Ramponi, P. Laporta, and S. De Silvestri, "Femtosecond micromachining of symmetric waveguides at 1.5 mm by astigmatic beam focusing," Opt. Lett. **27**, 1938–1940 (2002).

45. J. Burghoff, S. Nolte, and A. Tünnermann, "Origins of waveguiding in femtosecond laser-structured LiNbO₃," Appl. Phys. A **89**, 127–132 (2007).

46. G. A. Torchia, A. Rodenas, A. Benayas, E. Cantelar, L. Roso, and D. Jaque, "Highly efficient laser action in femtosecond-written Nd:yttrium aluminum garnet ceramic waveguides," Appl. Phys. Lett. **92**, 111103 (2008).

47. L. Li, W. J. Nie, Z. Q. Li, Q. M. Lu, C. Romero, J. R. Vázquez de Aldana, and F. Chen, "All-laser-micromachining of ridge waveguides in LiNbO₃ crystal for mid-infrared band applications," Sci. Rep. **7**, 7034 (2017).

48. H.-D. Nguyen, A. Ródenas, J. R. Vázquez De Aldana, G. Martín, J. Martínez, M. Aguiló, M. C. Pujol, and F. Díaz, "Low-loss 3D-laser-written mid-infrared LiNbO₃ depressed-index cladding waveguides for both TE and TM polarizations," Opt. Express **25**, 3722–3736 (2017).

49. L. Li, W. Nie, Z. Li, C. Romero, R. I. Rodriguez-Beltrán, J. R. Vázquez De Aldana, and F. Chen, "Laser-writing of ring-shaped waveguides in BGO crystal for telecommunication band," Opt. Express **25**, 24236–24241 (2017).

50. S. Kroesen, W. Horn, J. Imbrock, and C. Denz, "Electro–optical tunable waveguide embedded multiscan Bragg gratings in lithium niobate by direct femtosecond laser writing," Opt. Express **22**, 23339–23348 (2014).

51. H.-D. Nguyen, A. Ródenas, J. R. Vázquez de Aldana, J. Martínez, F. Chen, M. Aguiló, M. C. Pujol, and F. Díaz, "Heuristic modelling of laser

written mid-infrared LiNbO₃ stressed-cladding waveguides," Opt. Express **24**, 7777–7791 (2016).

52. O. Caulier, D. Le Coq, E. Bychkov, and P. Masselin, "Direct laser writing of buried waveguide in As₂S₃ glass using a helical sample translation," Opt. Lett. **38**, 4212–4215 (2013).

53. G. Salamu, F. Jipa, M. Zamfirescu, and N. Pavel, "Cladding waveguides realized in Nd:YAG ceramic by direct femtosecond-laser writing with a helical movement technique," Opt. Mater. Express **4**, 790–797 (2014).

54. Q. Zhang, D. Yang, J. Qi, Y. Cheng, Q. Gong, and Y. Li, "Single scan femtosecond laser transverse writing of depressed cladding

waveguides enabled by three-dimensional focal field engineering," Opt. Express **25**, 13263–13270 (2017).

55. C. Yan, S.-J. Huang, Z. Miao, Z. Chang, J. Z. Zeng, and T. Y. Wang, "3D refractive index measurements of special optical fibers," Opt. Fiber Technol. **31**, 65–73 (2016).

56. J. R. Grenier, L. A. Fernandes, and P. R. Herman, "Femtosecond laser writing of optical edge filters in fused silica optical waveguides," Opt. Express **21**, 4493–4502 (2013).

57. C. W. Smelser, S. J. Mihailov, and D. Grobnic, "Formation of Type I-IR and Type II-IR gratings with an ultrafast IR laser and a phase mask," Opt. Express **13**, 5377–5386 (2005).